Eur. Phys. J. A **17**, 49–56 (2003)
DOI 10.1140/epja/i2002-10139-0

THE EUROPEAN PHYSICAL JOURNAL A

Fission lifetimes of Th nuclei measured by crystal blocking

S.A. Karamian[1], J.S. Forster[2], J.U. Andersen[3,a], W. Assmann[4], C. Broude[5], J. Chevallier[3], J.S. Geiger[2], F. Grüner[4], V.A. Khodyrev[6], F. Malaguti[7], and A. Uguzzoni[7]

[1] FLNR JINR, 141980 Dubna, Russian Federation
[2] Départment de Physique, Université de Montréal, Montréal, Quebec, H3C 3J7 Canada
[3] Department of Physics and Astronomy, University of Aarhus, DK-8000 Aarhus C, Denmark
[4] Sektion Physik, Universität München, 85748 Garching, Germany
[5] Physics Department Weizmann Institute of Science, Rehovot, Israel
[6] Moscow State University, Moscow, Russian Federation
[7] Department of Physics, University of Bologna and INFN Bologna, Italy

Received: 2 October 2002 / Revised version: 1 January 2003 /
Published online: 29 April 2003 –
Communicated by J. Äystö

Abstract. Crystal blocking lifetime measurements have been made for highly excited Th nuclei with neutron number well removed from the stability line. Thin W crystals were bombarded with ^{32}S ions in the energy range 170–180 MeV and the yield of fission fragments was measured for emission close to a $\langle 111 \rangle$ axis. The fission blocking dips are compared to the appropriately scaled ones for elastic scattering of the ^{32}S beam ions and no significant difference is seen between the dips. This implies that the fraction of nuclei fissioning with lifetimes longer than 10 as is less than 2%. Fission lifetimes are increased by viscosity in the nuclear mass flow and comparison with a statistical model calculation indicates that the viscosity parameter, η, must be lower than for Th and U nuclei near β-stability. The effect of the $N = 126$ magic number is discussed.

PACS. 24.75.+i General properties of fission – 61.85.+p Channeling phenomena (blocking, energy loss, etc.)

1 Introduction

Crystal blocking is a time-of-flight technique based on blocking in the direction of a crystal axis of charged particles from a nuclear decay at a lattice site [1]. The blocking dip in the angular distribution is filled in if, due to the recoil in the reaction, the decaying nucleus is displaced from the lattice site by more than ~ 0.1 Å. The technique has been used for measuring lifetimes of highly excited compound nuclei preceding heavy-ion–induced fission since the early 1970s [2–7] when relatively long lifetimes ($\tau > 10^{-17}$ s) were observed for excitation energies between 50 and 100 MeV in the compound nucleus. The blocking dips were analysed in terms of two lifetime components, one very short ($< 10^{-17}$ s) and one long ($\sim 10^{-16}$ s), and statistical model calculations revealed that the long-lived component was the result of the latter stages of multi-chance fission [6,7].

Since the mid 1980s the so-called "nuclear clock" methods [8] have been applied in which the time scale of fission is deduced from the number of pre-scission neutrons, light charged particles or giant-dipole gamma-rays (GDR). Times deduced from GDR measurements were in order of magnitude agreement with the blocking results, while the average time deduced from the number of pre-scission neutrons was significantly shorter than that deduced from crystal blocking [8]. However, as pointed out in [9] this apparent discrepancy resulted from an inconsistency in the definition of the fission delay. In the analysis of pre-fission neutron multiplicities only the neutron delay times but not the time of successful fission after neutron emission were included, and this resulted in the smaller values of the deduced fission delay. Another analysis was given in [10]. The consistency of the two methods has also been demonstrated by statistical model calculations which reproduced both the fission delays measured by blocking and experimental values of the average number of pre-scission neutrons [7].

In the early 1990s an "atomic clock" method was introduced in which the time scale for fission is compared with the time for filling of a K-shell vacancy in the compound atom [11]. The surprising result obtained was that an appreciable fraction of fission events from ^{238}U at excitation

[a] e-mail: jua@ifa.au.dk

energies as high as 100 MeV were delayed by at least the uranium K-vacancy lifetime of 7 as. This result has been supported by more recent blocking studies carried out at GANIL with 24 MeV/u beams of ^{238}U ions [12]. Fission was induced by deep-inelastic scattering in a thin Si crystal and blocking patterns were recorded for fission fragments at very small angles to the beam direction. The excitation energy in individual events was estimated from the recorded neutron multiplicity, and a significant filling-in of the blocking dips was observed for excitation energies up to 250 MeV. Recently the same group obtained similar results for lead nuclei [13].

It should be noted that the crystal blocking and atomic clock methods give time information directly and do not as the nuclear clock methods rely on nuclear models to determine lifetimes. The atomic clock method determines the fraction of decays with a delay longer than the lifetime of a K-shell vacancy thus dividing the decays into two distinct time regions. In the case of crystal blocking additional information on the time evolution is obtained. If the lifetime is well defined the filling-in of the blocking dip consists of both an increase of the minimum and a strong narrowing of the dip. On the other hand, a combination of events with very short and very long lifetimes gives a blocking dip with only an increased minimum and no narrowing [5].

In general the methods are most sensitive within restricted time regions, whereas the time distribution for multi-chance fission covers several orders of magnitude (from 10^{-20} to 10^{-16} s). The blocking method is most sensitive to the long-time component, typically $\tau > 10^{-17}$ s, and for a broad distribution in fission times it determines the fraction of decays with a long lifetime. The GDR gamma-ray time scale is restricted by the fact that the probability of emission of high-energy gamma-rays is drastically reduced at lower excitation energies. Indeed, assuming a significant yield of fission after emission of several neutrons, with the initial excitation energy of 50–70 MeV reduced to a residual excitation of 15–25 MeV, the long-time component should be large but the GDR "clock" will show a short lifetime because GDR gamma-rays are only observed from the first stages in the evaporation cascade. The "neutron clock" method, when applied correctly, can reflect the mean time scale for the bulk of the fission events but it is again not sensitive to a long tail of the time distribution. As a result, the comparison of time scales determined by nuclear clock methods with those obtained by the direct methods is not straightforward. One can compare the different methods through statistical model simulations since all the measured quantities can be calculated, *e.g.*, the neutron multiplicity, the GDR gamma intensity, the blocking minimum yield and the K-X-ray intensity. However, such a comparison is model dependent.

The observed long fission delays for highly excited ^{238}U nuclei have been attributed to a high viscosity in the nuclear mass flow, and the present work was undertaken to shed more light on this interesting aspect of nuclear dynamics. We have made blocking lifetime measurements for Th compound nuclei produced by the fusion-fission reaction: a W crystal was bombarded with beams of 170 to 180 MeV ^{32}S ions.

2 Experimental details

Historically, some criticism of the blocking method has been expressed. Questions have been raised concerning the fragment selection by solid-state track detectors, the role of dechanneling due to the finite crystal thickness, lattice damage induced by the beam, calibration of the blocking yield for zero lifetime, calculation of lifetimes from the measured parameters and distortion of the blocking dip by post-scission particle emission. Such problems are well accounted for today. For example, perfect crystals can be prepared with a thickness as small as 100 nm. It has been shown in separate experiments that even for such thin crystals an equilibrium blocking distribution is formed and dechanneling is negligible. The damage of W crystals has been studied in [14] and it was observed that doses as large as 10^{16} ions/cm^2 produce an additional yield in the blocking minimum of only about 1%. In the present experiment the beam spot was moved to a new position on the crystal each time the dose reached $\sim 10^{16}$ ions/cm^2. The high-precision goniometer allows translations without significant change of angles. Furthermore, the elastically scattered ions supplying the zero-lifetime calibration were recorded simultaneously. The event-mode recording also allows an investigation of possible damage effects in playback and a rejection of data recorded after too high a dose on one spot. Other questions are discussed in more detail below. The simulation procedures are also important and are described in sects. 4 and 5.

The measurements were made with ^{32}S beams of 170 to 180 MeV from the tandem accelerator of the University of Munich at Garching. Elastically scattered ^{32}S ions and fission fragments were detected in a large-solid-angle ionisation counter [15] with an entrance aperture of 8 cm by 8 cm. The anode of the detector is split into two electrodes. The first (12 cm long) gives a ΔE signal and the second (18 cm long) an $E_{\rm rest}$ signal and the total energy deposited in the counter is then the sum $\Delta E + E_{\rm rest}$. The detector has the capability to determine the position where the detected particle entered the counter. This is achieved with a cathode electrode in the shape of a backgammon, and the x-position is determined by the signals from the left (l) and right (r) sections as the ratio $(l-r)/(l+r)$. Since the signal measured at the cathode is dependent on the distance of the trajectory of the detected particle from the cathode (the closer to the cathode the bigger the signal) the y-position can be determined from the ratio of the cathode and anode signals, *i.e.*, as $(l+r)/(\Delta E + E_{\rm rest})$.

The split anode provides a means of particle identification from a plot of ΔE *vs.* $E_{\rm rest}$, as shown in fig. 1 for a 170 MeV ^{32}S beam on the crystal target and a gas pressure of 25 Torr isobutane in the counter. The region of the plot corresponding to fission fragments from Th compound nuclei is marked. Since the pressure in the counter is low the light products such as elastically scattered ^{32}S

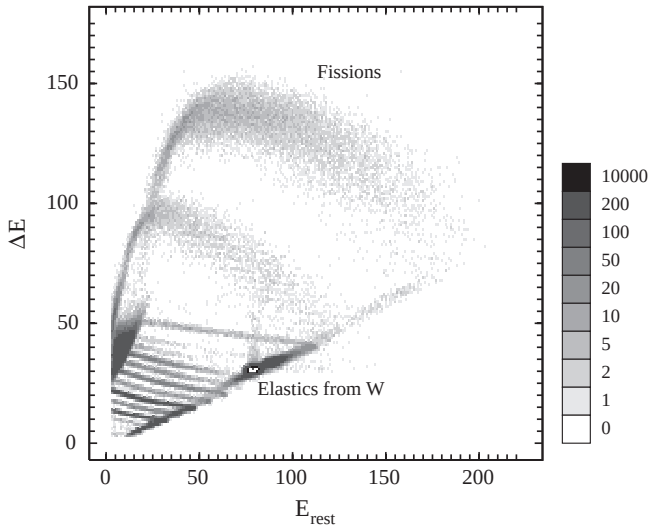

Fig. 1. ΔE *vs.* $E_{\rm rest}$ spectrum for a detector gas pressure of 25 Torr.

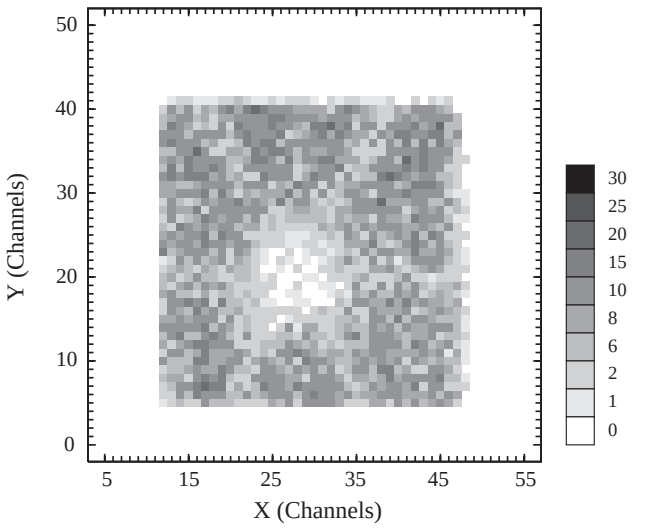

Fig. 2. Blocking pattern along a ⟨111⟩ axial direction for fission fragments from 170 MeV ^{32}S bombardment of a thin W crystal.

do not stop in the detector, and there is a folding back of the lines in the ΔE *vs.* $E_{\rm rest}$ plot. ^{32}S ions scattered elastically from W appear as a small circle in the 2d plot because of the small energy loss of the ^{32}S ions in the thin target. Other lines in fig. 1 come from particles emitted from reactions with the substrate.

The blocking lifetime measurements were made with 100 nm thick crystals of natural W grown epitaxially on a 200 nm thick crystal of Mo, which was, in turn, grown on an MgO substrate with a ⟨100⟩ axis normal to its surface. The crystal was oriented such that a ⟨111⟩ axis at 35° to the crystal surface was pointing at the detector. The ionisation detector was positioned at 50.2° to the beam direction with the result that the target was at 15.2° to the beam. Thus the full thickness of the W crystal is approximately 380 nm for the beam and 175 nm for fission fragments.

The event-by-event data consisting of ΔE, $E_{\rm rest}$, l and r signals were recorded on the hard disk of the data acquisition computer for later playback.

3 Data analysis

The event-by-event data were played back by first setting polygons on the fission and elastic regions in the ΔE *vs.* $E_{\rm rest}$ plot. For events in the fission and elastic polygons a 2d plot of x *vs.* y was generated as described above. Since the relationships yielding x and y prove to be non-linear the x-y plots had to be corrected for this non-linearity. The correction was based on a set of data taken with a mask placed in front of the detector. The mask, which has a 9 by 9 array of 1.0 mm diameter holes at 5.0 mm spacing, was placed 530 mm from the target. From the centroids of the "peaks" in the 2d mask data it is possible to correct the observed data so that it fits onto a square grid. This procedure also provides an angular calibration for the detector. The mask data were collected for elastically scattered ^{32}S ions only and since the y-coordinate also depends on the mass of the detected particle, we scaled the y-parameter for the fissions so that the axis of the fission and elastic blocking patterns occurred at the same y-coordinate. A typical 2d blocking pattern for fissions resulting from 170 MeV ^{32}S bombardment of the W crystal is shown in fig. 2. Both the ⟨111⟩ axis and the {110} planes are clearly seen.

Experimental blocking patterns were obtained from circular averages about the central minimum in the two-dimensional position spectra. As pointed out earlier [6] this has the advantage of improving statistical accuracy as well as eliminating the influence of planar effects. Figure 3 shows elastic and fission blocking patterns for 170, 175 and 180 MeV bombarding energies. The uncertainties are statistical only.

The FWHM of the blocking dips are proportional to the Lindhard critical angle [16] for channeling, ψ_1, given by

$$\psi_1 = \left(\frac{2Z_1Z_2e^2}{Ed}\right)^{1/2}, \qquad (1)$$

where Z_1 and Z_2 are the atomic numbers of the particle and the crystal atoms, d is the atomic spacing along the axis and E is the particle energy. For a given crystal, Z_2 and d are constants and one can compare dips for different particles by $(Z_1/E)^{1/2}$ scaling. The elastically scattered ^{32}S ions represent a prompt process and the elastic dips have been scaled in width to that of the fission fragments to provide a zero-lifetime calibration, as seen in fig. 3. The average atomic number and energy of the fragments were used for the scaling according to eq. (1).

Inspection of the figure reveals that there is little difference between the fission and the scaled elastic dips at all three bombarding energies. The minimum yields, $\chi_{\rm min}$, given in table 1 were calculated from the counts in the centre of the dips, corresponding to the smallest three angles in fig. 3.

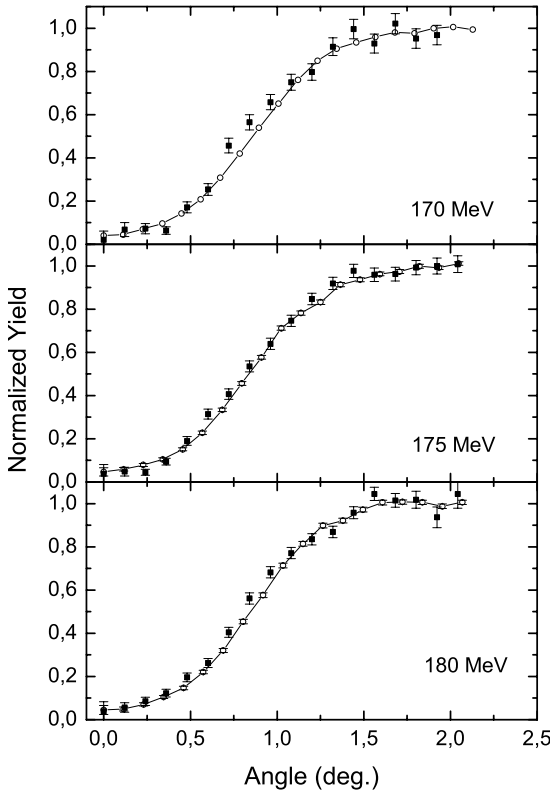

Fig. 3. Fission fragment blocking dips (closed squares) and scaled elastic scattering dips (open circles) for 170, 175 and 180 MeV ^{32}S bombardment of a thin W crystal.

Table 1. Parameters of the reaction and results of the experiment.

E_i(MeV)	170	175	180
$E^*_{\rm C}$ (MeV)	62	66	70
$I_{\max}$ ($\hbar$)	32	40	47
$\chi_{\min}$ (Fission)	0.062 (17)	0.046 (11)	0.070 (14)
$\chi_{\min}$(Elastic)	0.058 (5)	0.069 (5)	0.062 (5)
$\Delta\chi_{\min}$ (Exp.)	0.004 (18)	−0.023 (12)	0.008 (15)

4 Statistical model calculations

Statistical decay widths $\Gamma_{\rm n}$, $\Gamma_{\rm f}$ and Γ_γ were calculated for a Th compound nucleus with a mean mass number $A = 214$, which corresponds to an average over both the target isotopic composition and the number of evaporated neutrons. The mean neutron binding energy was taken to be $B_{\rm n} = 9$ MeV. One can show that the averaging of odd-even staggering in $B_{\rm n}$ values is equivalent to taking into account the pairing corrections in the level density. The lifetime of a nucleus at a given excitation energy and angular momentum is defined by the total width $\tau_{\rm tot} = \hbar/\Gamma_{\rm tot}$, where $\Gamma_{\rm tot} = \Gamma_{\rm n} + \Gamma_{\rm f} + \Gamma_\gamma$. The emission of charged particles has a much lower probability and was neglected in the present calculations. The differential fission probability is expressed via the width ratio $\Gamma_{\rm f}/\Gamma_{\rm tot}$. The total fission probability then appears as an additive sum of all fission chances:

$$P_{\rm f}({\rm tot}) = \sum_{I=0}^{I_{\max}} \frac{\sigma_I}{\sigma_{\rm c}} \sum_{x=0}^{x_{\max}} \frac{\Gamma_{\rm f}}{\Gamma_{\rm tot}}\,(x,I) \prod_{k=0}^{x} \frac{\Gamma_{\rm n}}{\Gamma_{\rm tot}}\,(k,I)\,, \quad (2)$$

where I is the angular momentum of the fusion reaction, x is the number of emitted neutrons, σ_I and $\sigma_{\rm c}$ are partial and total cross-sections for the compound-nucleus (CN) formation.

The mean number of pre-fission neutrons is also expressed simply as

$$\nu_{\rm pre} = \frac{1}{P_{\rm f}({\rm tot})} \sum_{I=0}^{I_{\max}} \frac{\sigma_I}{\sigma_{\rm c}} \sum_{x=1}^{x_{\max}} x \cdot P_{x{\rm f}}\,(I), \quad (3)$$

where $P_{x{\rm f}}$ is the partial fission probability contained in eq. (2).

In our calculations we used standard statistical equations and the level density function $\rho(E^*, I)$ given by Gilbert and Cameron [17]. The width values have been calculated as a function of two parameters, the thermal excitation energy U and the angular momentum I:

$$U = E^* - E_{\rm R}, \quad (4)$$

where the rotational energy $E_{\rm R}(I)$ is calculated assuming a rigid-rotor moment of inertia.

For the CN the angular-momentum distribution, σ_I, was calculated in the standard barrier-penetration form with two parameters $I_{\max}$ and ΔI. The usual Weisskopf approach was applied to calculate the $\Gamma_{\rm n}$ values. It includes the product of the level density ρ and the neutron transmission coefficients T_ℓ integrated over the residual excitation energy and summed over the spin quantum numbers of the daughter nucleus. The expression used was

$$\Gamma_{\rm n}\,(E^*, I) = \frac{(2s+1)}{4\pi\,\rho_{\rm c}\,(E^*, I)} \times \sum_{\ell=0}^{\ell_{\max}} \sum_{j=I-\ell}^{I+\ell} \int_0^{E^*-B_{\rm n}-E_{\rm R}^{\min}} \rho_{\rm n}[(E^*-B_{\rm n}-\varepsilon)\,, j]\; T_\ell(\varepsilon){\rm d}\varepsilon, \quad (5)$$

where s and ℓ are the quantum numbers of the emitted neutron and ε is its kinetic energy. The neutron transmission coefficients T_ℓ were calculated in the black-nucleus model.

In the calculations it was found that the main influence of I on $\Gamma_{\rm n}$ (a reduction) arises due to the subtraction of the rotational energy $E_{\rm R}$ from E^*. The summation over the quantum numbers in eq. (5) introduces a rather weak second-order effect which is negligible for $U > 20$ MeV. We note that the approximate formula given by Moretto [18] gives the same result within 5% for $U > 25$ MeV. We further note that some authors assume that Γ_i is proportional to $\exp(-B_i/T)$ but this is too simplified and gives only a rough estimate for Γ_i.

The fission width $\Gamma_{\rm f}$ has been calculated using the standard Bohr-Wheeler approach and multiplied by the

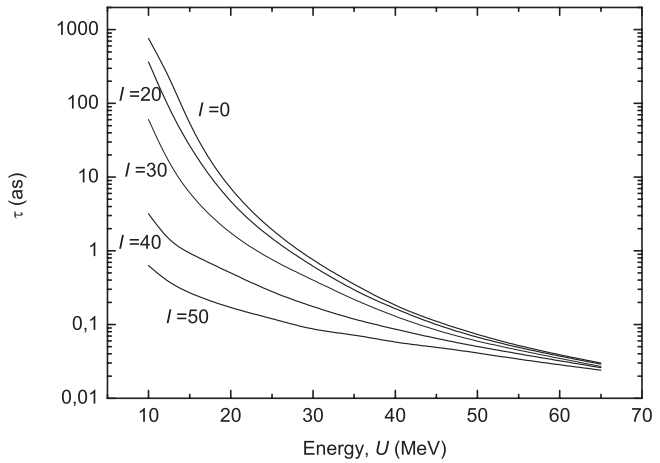

Fig. 4. CN lifetime calculated for ^{214}Th in the 3rd iteration with $\eta = 3.5$ (at 65 MeV) as a function of U and I. τ is a combination of three partial lifetimes corresponding to the neutron emission, fission and gamma-emission modes.

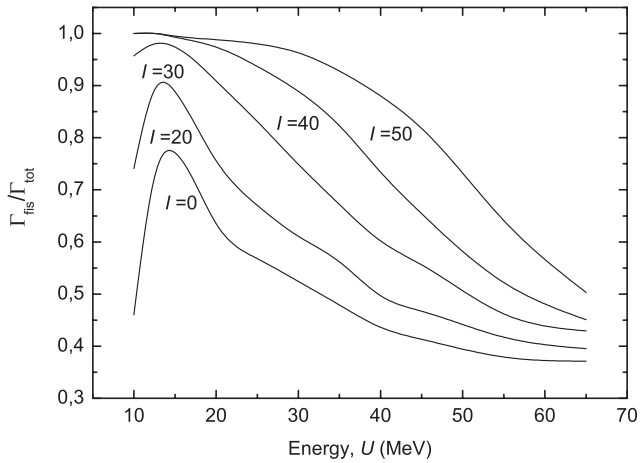

Fig. 5. Fission probability as a function of U and I, in the 3rd iteration for ^{214}Th.

Kramers factor, as follows:

$$\Gamma_{\rm f}\left(E^*, I\right) = \frac{\left(\sqrt{1+\eta^2}-\eta\right)}{2\pi\ \rho_{\rm c}\left(E^*, I\right)} \times \int_0^{E^*-B_{\rm f}(I)-E_{\rm R}(I)} \rho_{\rm f}[\left(E^*-B_{\rm f}(I)-\varepsilon\right), I]\,{\rm d}\varepsilon, \quad (6)$$

where $B_{\rm f}(I)$ is the angular-momentum–dependent fission barrier [19] and η is the combined friction, inertia, stiffness parameter [20]. The term η is responsible for the fission retardation due to the nuclear-matter viscosity, according to the classical work of Kramers [21].

For a quantitative choice of the fission barrier height we used the analysis of experimental data in [22–24]. For neutron deficient ^{214}Th ($Z^2/A = 37.9$) the value $B_{\rm f} = 7$ MeV is taken at $I = 0$. With increasing I it decreases according to [19] down to 2.5 MeV at $I = 50\hbar$. To check the correctness of this choice the $B_{\rm f}$ values have also been calculated with shell corrections included for each isotope of interest. Again the shell correction part of $B_{\rm f}$ decreases with E^* as shown in [25] and the liquid-drop part of the barrier height depends on I as given in [19]. In this model we found that $B_{\rm f}$ went from 8.5 MeV to 2 MeV for all isotopes and for all values of E^* and I in our reaction. One can see that the phenomenological choice is close to the results of more sophisticated calculations. Thus, for simplicity, the phenomenological $B_{\rm f}(I)$ values have been used in our calculations.

The total width for electromagnetic decay, Γ_γ, is proportional to the cube of the excitation energy if the GDR strength is used. Thus, we assumed $\Gamma_\gamma \propto U^3$ with normalisation to the width systematics for neutron resonances. Γ_γ is comparable to $\Gamma_{\rm n}$ and $\Gamma_{\rm f}$ only for U values near 10 MeV and below.

The level density parameters characterising the compound nucleus near static deformation and the daughter nucleus after neutron emission have been chosen as $a_{\rm c} = a_{\rm n} = A/10$ MeV^{-1}. For fission, a higher level density at the saddle point is normally assumed. We therefore assumed that $a_{\rm f}$ (I) follows the fission-barrier spin dependence, varying from 1.07 $a_{\rm n}$ at $I = 0$ to 1.0 $a_{\rm n}$ at $I = 50\hbar$.

Three sets of calculations have been carried out within the scheme described above. The parameters were fixed except for the dimensionless friction parameter η. We first assumed $\eta = 0$ but this resulted in too high a probability for fission, while the pre-fission neutron emission and evaporation residue cross-sections were much smaller than those expected from experimental results. We then changed the value to $\eta = 7$ at $E^* = 65$ MeV and decreasing linearly with decreasing E^*. This choice was based on the results of [26–28] but it results in a large long-lived component in contradiction to our measurements. Finally, in a third iteration the η-parameter was reduced by a factor of 2 (to $\eta = 3.5$) and this gives a long-lived component consistent with the blocking yield observed in our experiment.

The main parameters of the reaction and the experimental results are given in table 1 and the results of the simulations from the last two iterations in table 2. In figs. 4 and 5 the calculated lifetime $\tau_{\rm tot}$ and fission probability are shown as functions of thermal excitation energy and angular momentum for a ^{214}Th compound nucleus. One can see the very strong influence of the angular momentum on the basic decay properties and this influence is due to the $\Gamma_{\rm f}(I)$-dependence. We stress that our calculations are similar to many other statistical analyses described in the literature. In principle, the same approach and similar parameters are used. The only difference in our calculations is that we tried to follow the low-intensity tails in the time distribution of the fission events.

5 Details of the simulation

The results shown in figs. 4 and 5 are not sufficient to simulate the intensity of the long-lived fission component. One needs to calculate the time distribution of fission events

Table 2. Results of simulations, $2^{\rm nd}/3^{\rm rd}$ iteration.

$P_{\rm f}$ total	0.957/0.995	0.979/0.996	0.987/0.998
$\nu_{\rm pre}$	1.60/1.07	1.61/1.02	1.57/0.99
Relative yield (4nf)	0.107/0.040	0.086/0.032	0.075/0.029
Relative yield (5nf)	0.005/0.003	0.028/0.006	0.032/0.010
Partial yield of $t > 10$ as events	0.064/0.029	0.041/0.017	0.021/0.010
$\Delta\chi_{\rm min}$ (Blocking simulation)	0.040/0.019	0.031/0.014	0.010/0.005

taking into account all possible chances for fission, their probability and the corresponding parameters of residual excitation energy and angular momentum. For a Weisskopf spectrum of neutrons, each neutron emission leads on the average to subtraction of $(B_{\rm n} + 2T)$ from the excitation energy. The value $2T$ corresponds to the mean kinetic energy of the neutron and the temperature parameter has been calculated using the Fermi-gas equation: $a_{\rm n}T^2 = (U - B_{\rm n})$. The emission of a neutron leads also to a decrease of the CN angular momentum by about $1.5\hbar$ and to a dispersion of the distribution in E^* and I, and this was taken into account in our analytical approximation. A more accurate calculation would require a multi-coordinate Monte Carlo program. For our purpose, the approximations were adequate to vary the value of the parameter η in order to obtain agreement with the blocking results and, at the same time, reproduce satisfactorily the measured evaporation residue cross-section.

The mean fission lifetime after emission of x neutrons can be written as

$$\tau_\Sigma\,(x, I) = \sum_{k=0}^{x} \tau\,(k, I)\,. \tag{7}$$

The probability distribution $\mathrm{d}W/\mathrm{d}\tau_\Sigma$ has been calculated including all chances of fission and the τ distribution calculated at each chance. In the first steps for $x = 0$, 1, 2 neutrons the distributions can be characterised by the probability of the chance and by the mean lifetime only. As more neutrons are emitted and E^* decreases the τ-function becomes steeply dependent on the residual E^* and I. Thus, the variation of τ within a separate chance is significant and the probability distribution is not characterised by a single mean value of τ_Σ but by a distribution in τ_Σ.

The next stage of the calculations produces the distribution of the real decay time t. The "decay curve" $\mathrm{d}N_{\rm f}/\mathrm{d}t$ has been calculated as a superposition of many exponential components,

$$\frac{\mathrm{d}N_{\rm f}}{\mathrm{d}t} = c \int_0^\infty e^{-t/\tau_\Sigma}\ \frac{\mathrm{d}W}{\mathrm{d}\tau_\Sigma}\ \mathrm{d}\tau_\Sigma. \tag{8}$$

The constant c normalises the total number of events $N_{\rm f}$ to unity. In the numerical calculations the integral has been replaced by the sum and the infinity limit is replaced by 10^{-16} s. At longer times γ-decay competes with neutron emission and fission.

In fig. 6 the calculated time distributions (for the 3rd iteration) for $^{\rm nat}$W(^{32}S, f) reactions are shown corresponding to projectile energies of 170, 175 and 180 MeV. It is seen that the distribution covers a wide time range and it could not be approximated by a combination of 2-3 exponentials. The tails of the distributions are not very intense for $\eta = 3.5$ but they are not negligible.

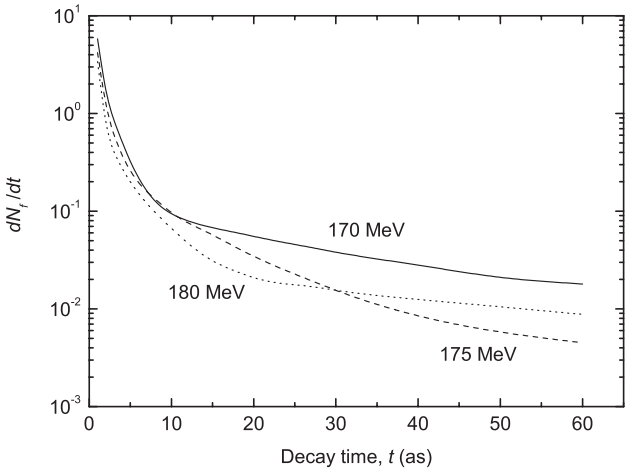

Fig. 6. Time distribution of fission events for the $^{\rm nat}$W(^{32}S, f) reaction at projectile energy values of 170, 175 and 180 MeV (eq. (8)). Simulation in the 3rd iteration.

To compare the statistical simulations with the blocking results another set of calculations is required. The calculated time distributions should be inserted into a code specifically developed for the simulation of charged-particle transmission through a single crystal. Several such codes exist and they reproduce successfully almost all properties of channeling and blocking effects. In particular, the UPIC code [29] calculates the trajectories of ions in a crystal lattice from binary collisions with the ordered atoms. Thermal vibrations, energy loss and multiple scattering are taken into account. Simulations with this code have been made for our cases.

The delayed-fission events shown in fig. 6 occur for a finite displacement of the emission point from the lattice site. Since the velocity and direction of the recoiling CN are known, the time scale can be linearly transformed to a displacement scale. The UPIC code was used with the time distributions shown in fig. 6 for the 2nd and 3rd iterations. The case of zero lifetime was also calculated for the comparison. The difference between minimum yields observed for finite times and for zero time, $\Delta\chi_{\rm min} = \chi_{\rm min}(t \neq 0) - \chi_{\rm min}(t = 0)$, is the lifetime effect from the calculations. It is given in table 2 and should be compared with the difference between the $\chi_{\rm min}$ values for

fission fragments and for the elastic scattering observed in the experiment, given in table 1. The statistical uncertainty on $\Delta\chi_{\min}$ is about a factor of five smaller in the simulations than in the experiment.

6 Discussion

Taking into account statistical errors only we deduce an experimental upper limit for $\Delta\chi_{\min}$ of 2% (table 1). This is in agreement with the results of the simulation in the 3rd iteration (fig. 6). As can be seen in table 2, the 2nd iteration with a friction parameter twice as large gives $\Delta\chi_{\min}$ values above 2% at 170 and 175 MeV. Thus, we conclude that the values of the friction parameter assumed in the 3rd iteration ($\eta = 3.5$ at $U = 65$ MeV) are realistic or play the role of an upper limit for friction in the $^{\rm nat}$W(^{32}S, f) reaction at projectile energies of 170–180 MeV. The total fission probability is very close to unity in agreement with the evaporation residue cross-section known from experiments.

The null result of our experiment thus indicates that the friction parameter is not very large. Due to the uncertainty of other parameters, we cannot claim to have set a strict limit on η but it is interesting that our finding is in qualitative agreement with recent results of Back *et al.* [30]. They measured evaporation residues for the same reaction as we used, namely ^{32}S bombardment of ^{184}W, from 165 to 257 MeV bombarding energy. In order to reproduce the measured residue cross-sections they needed an η value much lower than that for the Th nuclides of higher mass numbers with $A = 224$ and near $A = 232$ studied earlier. They relate this to the closed neutron shell at $N = 126$ and note that similar results are obtained for ^{3}He bombardment of ^{208}Pb which leads to a compound nucleus with $N = 127$. In contrast, for ^{16}O bombardment of ^{208}Pb leading to ^{224}Th with $N = 134$, well away from the $N = 126$ closed shell, they find a much stronger variation, from $\eta = 0$ at 40 MeV excitation and increasing linearly up to $\eta = 8$ at 80 MeV excitation. It would therefore be interesting to extend the blocking lifetime measurements to a compound system far from closed shells, *e.g.*, by ^{48}Ti bombardment of W.

Our limitation on the friction parameter is also significant in comparison with other results [12,28]. The long-lived fission component observed in [12] for fission of ^{238}U-like nuclei may indicate a large value for the friction parameter. Much shorter times were observed for ^{208}Pb-like nuclei [13] but these results were explained with a different theoretical approach [31] so a direct comparison is difficult.

More experiments are necessary to clarify the influence of shell effects on the friction parameter η. Some doubts arise because in heavy-ion–induced fission the effects are averaged over a wide range of deformation parameters, excitation energy and angular momentum for the nuclei under study.

Finally, we address a concern raised in the papers of the GANIL group [12,13] regarding the effect of post-scission neutron emission on the blocking dip. The recoil momentum changes the direction of motion of fission fragments and if the neutrons are emitted after the fragments have moved away from the $\langle 111\rangle$ atomic string containing the compound nucleus undergoing fission, the smearing of the angular distribution by such changes will fill in the blocking dip. On the other hand, neutron emission at recoil distances less than about 0.1 Å from an atomic string will not affect the blocking dip. The effect of secondary decay in blocking has been considered also by some of the present authors [32,33].

As a historical note we may add that before the interpretation of the results in [5–7] in terms of multi-chance fission was established, an explanation of the observed filling-in of fission blocking dips as an effect of delayed neutron emission from the fission fragments was suggested to us by a colleague, Dr F. Brown from Chalk River Labs, Canada. Our estimates indicated that this effect was small, and this was supported by our observation of fission dips nearly identical to the scaled elastic dip for some bombarding energies, since it is known that the emission of post-scission neutrons depends very weakly on bombarding energy.

We have simulated this effect in the present case assuming that the last post-scission neutron is emitted from a fragment with excitation energy evenly distributed from $B_{\rm n} + 1$ MeV to twice this energy. In this range, the lifetime varies from a few times 10^{-16} s to less than 10^{-18} s where the recoil distance is below 0.1 Å and hence the recoils from previous emission of neutrons at even shorter times can be neglected. For calculations with the UPIC code we find that changes to the dip are very small with only a slight narrowing and no significant increase in the minimum yield. Thus the effect is much smaller than indicated in [12]. There are two reasons for this: first, the lifetime for the emission of the last neutron was assumed to be 10^{-16} s in [12] and we find that the lifetime is usually much shorter. Second, the effect is much smaller for blocking along a $\langle 111\rangle$ axis in W than for a $\langle 110\rangle$ axis in Si because the critical angle in eq. (1) is larger by nearly a factor of three for the same values of Z_1 and E. The energy of the fission fragments was much larger in the experiments reported in [12] but this should not matter since the changes in angle due to neutron recoil and the critical angle ψ_1 both scale with $E^{-1/2}$. We conclude that the effects of recoil from post-scission neutron emission should be negligible in the present experiments. Similar conclusions were reached for the experiments in [2–7].

7 Conclusions

We have measured fission blocking distributions for ^{32}S bombardment of a thin W crystal at bombarding energies from 170 to 180 MeV. We have simultaneously measured the blocking patterns for elastically scattered ^{32}S ions and, when scaled in angle, these patterns provide a zero-lifetime reference. Within the statistical uncertainties the fission and elastic blocking dips are found to be identical, indicating that the fraction of fission processes occurring after 10^{-17} s is less than $\sim 2\%$.

The time distribution of fission events has been simulated in a statistical approach and the blocking profile evaluated with a binary-collision Monte Carlo code for the calculation of fragment trajectories in the lattice. The distribution covers a wide range of time, from 10^{-20} to 10^{-16} s, and we have discussed the consequences of this broad distribution for the comparison between different methods for the determination of the time scale of fission reactions.

The experimental results are compared to statistical model calculations incorporating a nuclear viscosity parameter η. A large viscosity increases the fraction of delayed, late-chance fission and our results indicate that η is not very large. This could be related to the fact that the neutron numbers for the compound nuclei are close to the magic number 126.

This work was supported by a grant from the Danish National Research Foundation to Aarhus Center for Atomic Physics (ACAP) and within the German-Russian Project DLR No. RUS-680-99. We are pleased to acknowledge support through NATO Grant 960122. We gratefully acknowledge valuable discussions with H. Hofmann and A.S. Jensen.

References

1. W.M. Gibson, Annu. Rev. Nucl. Sci. **25**, 465 (1975).
2. S.A. Karamian, Yu.Ts. Oganessian, F. Normuratov, Yad. Fiz. **14**, 499 (1971).
3. V.V. Kamanin, S.A. Karamian, F. Normuratov, S.P. Tretyakova, Yad. Fiz. **16**, 447 (1972).
4. V.N. Bugrov, S.A. Karamian, Yad. Fiz. **40**, 857 (1984).
5. J.U. Andersen, E. Lægsgaard, K.O. Nielsen, W.M. Gibson, J.S. Forster, I.V. Mitchell, D. Ward, Phys. Rev. Lett. **36**, 1539 (1976).
6. J.U. Andersen, A.S. Jensen, K. Jørgensen, E. Laegsgaard, K.O. Nielsen, J.S. Forster, I.V. Mitchell, D. Ward, W.M. Gibson, J.J. Cuomo, Mat.-Fys. Medd. K. Dan. Vidensk. Selsk. **40**, No. 7 (1980).
7. J.S. Forster, I.V. Mitchell, J.U. Andersen, A.S. Jensen, E. Laegsgaard, W.M. Gibson, K. Reichelt, Nucl. Phys. A **464**, 497 (1987).
8. D. Hilscher, H. Rossner, Ann. Phys. (Paris) **17**, 471 (1992) and references therein.
9. P. Paul, M. Thoennessen, Annu. Rev. Nucl. Part. Sci. **44**, 65 (1994).
10. K. Siwek-Wilczinska, J. Wilczinski, R.H. Siemssen, H.W. Wilshut, Phys. Rev. C **51**, 2054 (1995).
11. J.D. Molitoris, W.E. Meyerhof, Ch. Stoller, R. Anholt, D.W. Spooner, L.G. Moretto, L.G. Sobotka, R.J. McDonald, G.J. Wozniak, M.A. McMahon, L. Blumenfeld, N. Colonna, M. Nessi, E. Morenzoni, Phys. Rev. Lett. **70**, 537 (1993).
12. F. Goldenbaum, M. Morjean, J. Galin, E. Liênard, B. Lott, Y. Pêrier, M. Chevallier, D. Dauvergne, R. Kirsch, J.C. Poizat, J. Remillieux, C. Cohen, A. L'Hoir, G. Prêvot, D. Schmaus, J. Dural, M. Toulemonde, D. Jacquet, Phys. Rev. Lett. **82**, 5012 (1999).
13. F. Barruè, S. Basnary, A. Chbihi, M. Chevallier, C. Cohen, D. Dauvergne, H. Ellmer, J. Franckland, D. Jacquet, R. Kirsch, P. Lautesse, A. L'Hoir, M. Morjean, J.C. Poizat, C. Ray, M. Toulemonde, Nucl. Instrum. Methods B **193**, 852 (2002).
14. H. Huber, W. Assmann, S.A. Karamian, H.D. Mieskes, H. Nolte, E. Gazis, M. Kokkoris, S. Kossionides, R. Vlastou, R. Groetzschel, A. Mueklich, W. Prusseit, Nucl. Instrum. Methods B **146**, 309 (1998).
15. W. Assmann, H. Huber, C. Steinhauser, M. Dobler, H. Gluckler, A. Weidinger, Nucl. Instrum. Methods B **89**, 131 (1994).
16. J. Lindhard, Mat.-Fys. Medd. K. Dan. Vidensk. Selsk. **34**, No. 14 (1965).
17. A. Gilbert, A.G.W. Cameron, Can. J. Phys. **43**, 1446 (1965).
18. L.G. Moretto, Nucl. Phys. A **180**, 337 (1972).
19. S. Cohen, F. Plasil, W.J. Swiatecki, Ann. Phys. (N.Y.) **82**, 557 (1974).
20. H. Hofmann, D. Kiderlen, Phys. Rev. C **56**, 1025 (1997).
21. H. Kramers, Physica (Amsterdam) **7**, 284 (1940).
22. V.S. Barashenkov *et al.*, Part. Nucl. **5**, 479 (1974), in Russian.
23. M. Blann, D. Akers, T.A. Komoto, F.S. Dietrich, L.F. Hansen, J.G. Woodworth, W. Scobel, J. Bisplinghoff, B. Sikora, F. Plasil, R.L. Ferguson, Phys. Rev. C **26**, 1471 (1982).
24. M.C. Duijvestijn, A.J. Koning, F.J. Hambsch, Phys. Rev. C **64**, 014607 (2001).
25. A.V. Ignatiuk, G.N. Smirenkin, A.S. Tishin, Yad. Fyz. **21**, 485 (1975).
26. M. Thoennesen, D.R. Chakrabarty, M.G. Herman, R. Butsch, P. Paul, Phys. Rev. Lett. **59**, 2860 (1987).
27. D.J. Hofman, B.B. Back, P. Paul, Phys. Rev. C **51**, 2597 (1995).
28. I. Diószegi, N.P. Shaw, T. Mazumdar, A. Hatzikoutelis, P. Paul, Phys. Rev. C **61**, 024613 (2000).
29. V.A. Khodyrev, D.O. Boerma, Rad. Eff. Def. in Solids, **142**, 173 (1997).
30. B.B. Back, D.J. Blumenthal, C.N. Davids, D.J. Henderson, R. Hermann, D.J. Hofman, C.L. Jiang, H.T. Penttilä, A.H. Wuosmaa, Phys. Rev. C **60**, 044602 (1999).
31. I. Gontchar, M. Morjean, S. Basnary, Europhys. Lett. **57**, 355 (2002).
32. S.A. Karamian. Part. Nucl. **17**, 753 (1986), in Russian.
33. F. Malaguti, G. Giardina, P. Olivo, Nucl. Instrum. Methods B **129**, 341 (1997).